

Article

Semiconducting p-Type Copper Iron Oxide Thin Films Deposited by Hybrid Reactive-HiPIMS + ECWR and Reactive-HiPIMS Magnetron Plasma System

Zdenek Hubička ^{1,*} , Martin Zlámál ², Jiri Olejníček ¹, Drahoslav Tvarog ¹, Martin Čada ¹ and Josef Krýsa ^{2,*}

¹ Institute of Physics, Division of Optics, Academy of Sciences of the Czech Republic, Na Slovance 2, 182 21 Prague, Czech Republic; olejnj@fzu.cz (J.O.); tvarogd@fzu.cz (D.T.); cadam@fzu.cz (M.Č.)

² Department of Inorganic Technology, University of Chemistry and Technology Prague, Technická 5, 166 28 Prague, Czech Republic; zlamalm@vscht.cz

* Correspondence: hubicka@fzu.cz (Z.H.); krysj@vscht.cz (J.K.)

Received: 20 January 2020; Accepted: 25 February 2020; Published: 3 March 2020



Abstract: A reactive high-power impulse magnetron sputtering (r-HiPIMS) and a reactive high-power impulse magnetron sputtering combined with electron cyclotron wave resonance plasma source (r-HiPIMS + ECWR) were used for the deposition of p-type CuFe_xO_y thin films on glass with SnO_2/F conductive layer (FTO). The aim of this work was to deposit CuFe_xO_y films with different atomic ratio of Cu and Fe atoms contained in the films by these two reactive sputtering methods and find deposition conditions that lead to growth of films with maximum amount of delafossite phase CuFeO_2 . Deposited copper iron oxide films were subjected to photoelectrochemical measurement in cathodic region in order to test the possibility of application of these films as photocathodes in solar hydrogen production. The time stability of the deposited films during photoelectrochemical measurement was evaluated. In the system r-HiPIMS + ECWR, an additional plasma source based on special modification of inductively coupled plasma, which works with an electron cyclotron wave resonance ECWR, was used for further enhancement of plasma density n_e and electron temperature T_e at the substrate during the reactive sputtering deposition process. A radio frequency (RF) planar probe was used for the determination of time evolution of ion flux density $i_{ionflux}$ at the position of the substrate during the discharge pulses. Special modification of this probe to fast sweep the probe system made it possible to determine the time evolution of the tail electron temperature T_e at energies around floating potential V_{fl} and the time evolution of ion concentration n_i . This plasma diagnostics was done at particular deposition conditions in pure r-HiPIMS plasma and in r-HiPIMS with additional ECWR plasma. Generally, it was found that the obtained ion flux density $i_{ionflux}$ and the tail electron temperature T_e were systematically higher in case of r-HiPIMS + ECWR plasma than in pure r-HiPIMS during the active part of discharge pulses. Furthermore, in case of hybrid discharge plasma excitation, r-HiPIMS + ECWR plasma has also constant plasma density all the time between active discharge pulses $n_i \approx 7 \times 10^{16} \text{ m}^{-3}$ and electron temperature $T_e \approx 4 \text{ eV}$, on the contrary in pure r-HiPIMS n_i and T_e were negligible during the “OFF” time between active discharge pulses. CuFe_xO_y thin films with different atomic ration of Cu/Fe were deposited at different conditions and various crystal structures were achieved after annealing in air, in argon and in vacuum. Photocurrents in cathodic region for different achieved crystal structures were observed by chopped light linear voltammetry and material stability by chronoamperometry under simulated solar light and X-ray diffraction (XRD). Optimization of depositions conditions results in the desired Cu/Fe ratio in deposited films. Optimized r-HiPIMS and r-HiPIMS + ECWR plasma deposition at 500 °C together with post deposition heat treatment at 650 °C in vacuum is essential for the formation of stable and photoactive CuFeO_2 phase.

Keywords: photocathode film; r-HiPIMS + ECWR plasma; r-HiPIMS plasma; copper iron oxide; photocurrent

1. Introduction

Generally, highly efficient materials for photocathode thin film applied in solar water splitting cells are intensively searched. Key factors are low cost, high photoactivity and long-term stability. These materials should have suitable value of band gap E_g compatible with the solar spectrum, high absorption coefficient, p-type conductivity and good transport properties for photogenerated holes and electrons. One suitable candidate for efficient photocathode is Cu_2O with direct band gap $E_g = 2 \text{ eV}$ [1] and p-type conductivity. These Cu_2O films were used as effective photocathode in photoelectrochemical (PEC) cells but the stability problem was solved with additional layers ZnO:Al and TiO_2 made by atomic layer deposition (ALD) in order to improve stability during PEC measurement [2]. Because this approach is technologically complicated further approaches were tested. Some progress was achieved for films CuO . Cupric oxide CuO is p-type semiconductor material with band gap $E_g = 1.2\text{--}2.5 \text{ eV}$ and high absorption coefficient. CuO with increased stability was applied as photocathode and presented in reference [3]. In this work the improved stability was achieved with oxygen excess contained in films and with deposition of Au-Pd nanostructures on the surface of CuO films. Further approach for improvement PEC performance and stability of these photocathodes is to deposit CuFeO_2 with delafossite structure. This material has suitable band gap $E_g = 1.47 \text{ eV}$ and good stability in alkaline electrolytes which is used in PEC cells [4,5]. One of the problems with delafossite is the poor photoinduced electron-hole separation and charge collection [6]. Further improvement of PEC performance of this material is to deposit a $\text{CuFeO}_2/\text{CuO}$ composite structure with heterojunction between those two phases helping to improve PEC performance as photocathodes [7].

Recently, n-type semiconducting films applicable as photoanodes or suitable for photocatalytic application were deposited by the reactive DC, DC pulsed or RF magnetron sputtering as TiO_2 [8], Fe_2O_3 [9,10], TaON [11], WO_3 [12,13]. As photocathodes p-type semiconductor $\text{Cu}_2\text{O}/\text{CuO}$ thin film structures were prepared by reactive sputtering [14–16]. Further photocathodes thin films based on CuFeO_2 with p-type conductivity were prepared by RF sputtering [17].

Recently, reactive high-power impulse magnetron sputtering (r-HiPIMS) has become promising technology for various material preparation [18–25]. The magnetron discharge is generated in short pulses (10–100 μs) with low frequency of pulsing (100 Hz–1 kHz). The duty factor is very low in r-HiPIMS, and although the high power is applied in the discharge plasma in the active part of the pulse, the average applied power can be low with similar values like in classical DC magnetron sputtering [24]. This method relies on the intensive ionization of sputtered and reactively sputtered particles in high current discharge pulse [26–28], and the growing films is built from ions rather than from neutrals.

In order to extend possible conditions in r-HiPIMS plasma, a hybrid plasma source based on the combination of r-HiPIMS with RF inductively coupled plasma working in electron cyclotron wave resonance (ECWR) was developed [29–31] and tested for the deposition of TiO_2 textured rutile [32] and Fe_2O_3 with a hematite phase [33]. The possibility to operate the r-HiPIMS magnetron plasma at very low-pressure $p < 0.05 \text{ Pa}$, further increase of ionization of sputtered particles, higher electron temperature T_e during the active part of discharge pulse are great benefits of this hybrid r-HiPIMS + ECWR deposition system [31].

In this paper, the study of hybrid r-HiPIMS + ECWR plasma system and pure reactive r-HiPIMS with two magnetrons cathodes is presented together with RF probe plasma diagnostics during the deposition of copper iron oxide thin films. These films were investigated as photocathodes in a PEC solar water splitting system. The aim of this work was to deposit CuFe_xO_y films with different atomic ratio of Cu and Fe atoms contained in the films by these two reactive sputtering methods. The aim

was to study this ternary oxide for different molar ratio Cu and Fe contained in the film and to find deposition conditions which lead to growth of films with maximum amount of delafossite phase CuFeO_2 .

2. Experimental

Copper iron oxide thin films were deposited on fluorine doped tin oxide (FTO) conductive glass substrates. This is the glass substrate with 500 nm thick $\text{SnO}_2\text{:F}$ conductive layer with the sheet resistance $15 \Omega/\square$. The hybrid r-HiPIMS + ECWR deposition system can be seen in Figure 1. The reactor stainless steel chamber was continuously pumped by the turbomolecular (500 L s^{-1}) as a secondary pump and by the rotary vane pump ($25 \text{ m}^3\cdot\text{h}^{-1}$) as primary pump on the base pressure $p_b = 1 \times 10^{-4}$ Pa. Argon and oxygen gas flow Q_{Ar} and Q_{O_2} were fed into the reactor through the gas flow controller and the pressure p in the chamber was controlled during the deposition by the control gate valve and was held for all the deposition conditions on the value $p = 1$ Pa. Argon gas flow was held constant on the value $Q_{Ar} = 26$ sccm for all the deposition conditions. The gas flow of oxygen for particular conditions is shown in Table 1. The system was equipped with two magnetrons with circular planar cathodes with diameter 50 mm. The first cathode was made of pure iron (99.9%) with thickness 1.5 mm and the second one was made of pure copper (99.9%) with thickness 6 mm. The substrate was electrically floating and was placed 150 mm from the surface of both targets. The substrate was heated during the deposition with controlled temperature up to 500°C . The temperature of the substrate at particular deposition conditions are in Table 1. The substrate was rotating during the process with rotation speed 1 rpm. The water-cooled RF ICP coil was placed between magnetrons and the substrate (Figure 1). The diameter of the ICP coil was 200 mm, and the length was 120 mm. The power fed to this ICP coil was P_{ECWR} , and the values for particular conditions are in Table 1. The DC magnetic field was set to take the system as close as to ECWR resonance and the magnetic field was around $B \approx 1.7$ mT. Deposition time was always 60 min for all the deposited samples.

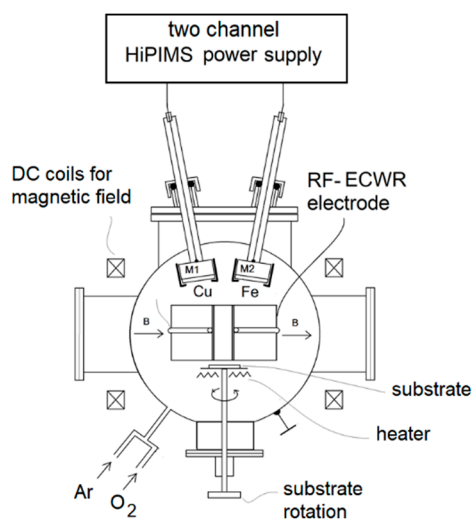


Figure 1. Experimental apparatus with two magnetrons and the radio frequency (RF) electron cyclotron wave resonance (ECWR) electrode for the deposition of copper iron oxide thin films.

Typical r-HiPIMS and r-HiPIMS + ECWR discharge waveforms are synchronized and can be seen in Figures 2 and 3, respectively. The length of pulses, their relative positions, and their pulsing frequencies were held constant for all investigated conditions. The “ON” time on the iron cathode was $T_{ONFe} = 100 \mu\text{s}$, and the “ON” time on the copper cathode was $T_{ONCu} = 20 \mu\text{s}$ for samples 5x–10x (Table 1). $T_{ONCu} = 30 \mu\text{s}$ for the sample 4x, 3x, $T_{ONCu} = 100 \mu\text{s}$ for the sample 2x and $T_{ONCu} = 50 \mu\text{s}$ for the sample 1x. The pulsing frequency on both cathodes was always $T_p = 100$ Hz.

Table 1. List of films with significant deposition parameters.

Sample	I_{Feav} [mA]	U_{Fe} [V]	I_{Cuav} [mA]	U_{Cu} [V]	Q_{O2} [sccm]	$t_{dep.}$ [°C]	Thickness [nm]	mol. Ratio Cu/Fe	P_{ECWR} [W]
1x	500	720	84	975	10	250	900	4.77	180
2x	500	720	176	1000	10	250	2200	12.35	180
3x	600	720	56	1000	10	250	580	4.27	180
4x	500	720	50	895	5	250	535	1.79	180
5x	550	600	40	841	5	250	250	1.33	180
6x	440	700	42	834	2	500	350	0.82	0
7x	400	700	47	816	1.3	500	600	0.82	0
8x	500	700	44	842	3.2	500	300	0.79	0
9x	500	700	40	804	2	500	400	0.94	0
10x	500	700	30	789	2	500	240	0.86	0

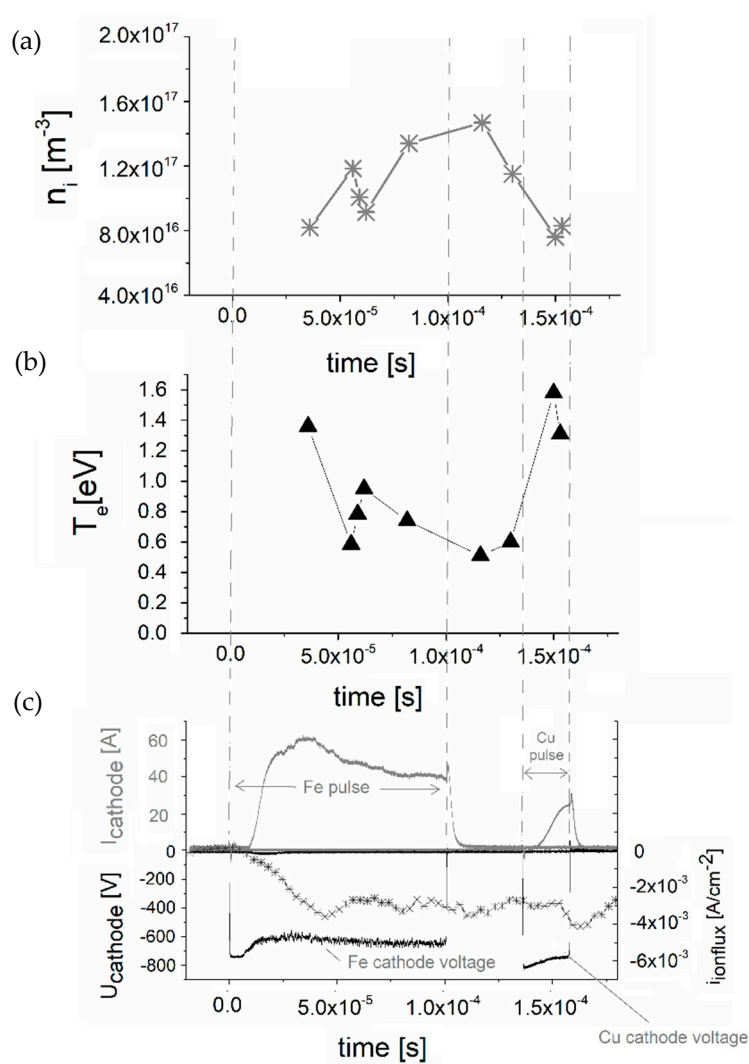


Figure 2. Time evolution of plasma parameters like, ion plasma density n_i (a), tail electron temperature T_e (b) and ion flux density on the probe $i_{ionflux}$ (c) of reactive r-HiPIMS without applied ECWR RF power.

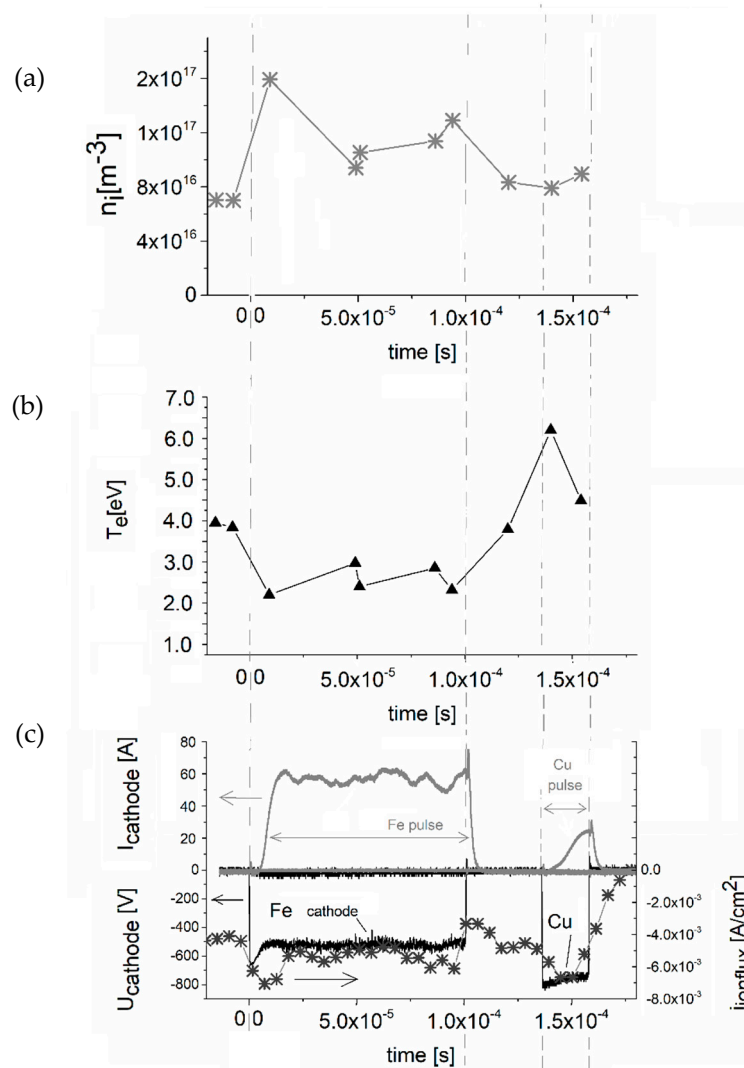


Figure 3. Time evolution of plasma parameters like ion plasma density n_i (a), tail electron temperature T_e (b) and ion flux density on the probe $i_{ionflux}$ (c) of reactive r-HiPIMS + ECWR plasma with applied RF power $P_{RF} = 180$ W.

Other discharge conditions like average iron cathode discharge current I_{Feav} , and average copper cathode current I_{Cuav} , copper or iron cathode voltage U_{Fe} , and copper cathode voltage U_{Cu} are mentioned in Table 1.

Transmission spectra of selected deposited films on FTO glass were measured by spectrometer (Carry 100, Varian, Palo Alto, CA, USA) with integrating sphere in the spectral range 200–900 nm.

The thickness of the films was determined by profilometry measurements (Alpha-Step 500 KLA Tencor MDL. no. ASIQ, San Jose, CA, USA). The deposited films were analyzed by X-ray diffraction (XRD). XRD data were measured at room temperature on a Bruker AXS D8 powder diffractometer (Billerica, MA, USA) in a Bragg-Brentano geometry using a $\text{CoK}\alpha$ radiation wavelength ($\lambda = 1.7903$ Å, $U = 34$ kV, $I = 30$ mA). Chemical composition regarding molar ratio of Cu/Fe was measured by XRF. ED-XRF spectrometer Niton XL5 (Thermo Scientific, Waltham, MA, USA) equipped with Ag anode X-Ray Tube (6–50 kV, 0–500 μA , max 5 W) was used. Measure area diameter was 3 mm. Niton Connect PC software (Version 1.0) was used for evaluation of the measured data.

In order to get a good and high-quality crystalline structure, the films were annealed after the deposition in air, argon or in high vacuum. A long annealing for 6 h in argon atmosphere on temperature 600 °C was already used for these CuFeO_2 delafossite films prepared by the RF reactive

co-sputtering, as reported in reference [17]. In our experiments, the annealing was done for selected samples in the air atmosphere. Temperature increase rate 10 °C/min to the temperature 650 °C with 3 h retention, and slow cooling (1 °C/min) was used. These conditions were found to be optimal by several preliminary experiments. Also, some samples received annealing in the high vacuum or in the argon directly in the plasma reactor after the deposition. A temperature of 500 or 650 °C and prolonged time of 6 h were used to provide enough time for crystallization process and formation of new crystalline phases in the material under high vacuum conditions.

Photoelectrochemical (PEC) measurements were done by the use of potentiostat (VoltaLAB PGZ100, RadiometerAnalytical SAS, Villeurbanne, France), connected to the three-electrode optical cell filled with 0.1 M Na₂SO₄ (pH = 5.8) electrolyte. All experiments were done under an air atmosphere. The sample, with irradiated area set to 1 cm² by Teflon tape, was connected as working electrode. Platinum sheet was used as counter electrode and Ag/AgCl in 3 M KCl ($E_{Ag/AgCl} = 0.207$ V) as reference electrode. All potentials reported in our text are related to the mentioned reference electrode. Linear sweep voltammetry (+200 to −600 mV, sweep rate 10 mV/s) was done under the pulsed modulated light illumination with 5 s intervals of light and dark. The light was modulated by an electronic controlled mechanical shutter. Chronoamperometry (at −400 mV) was done under continuous illumination after short 30 s dark conditioning. A solar simulator (Newport, Irvine, CA, USA), emitting artificial AM1.5G solar spectrum with the intensity 100 mW·cm^{−2}, was used as the light source.

Plasma Diagnostics by RF Planar Probe

Plasma diagnostics at conditions of reactive r-HiPIMS and r-HiPIMS + ECWR depositions were done by a so-called RF planar probe, which is described in detail in reference [34]. This method has origin in Sobolewski method presented in reference [35–37]. The detailed experimental description together with Figures S1–S4 are in the Supplementary Materials. The plasma diagnostics with the RF planar probe is presented in this paper just for two selected types of plasma generation. The first measured type is the pure reactive r-HiPIMS without applied RF power to ECWR electrode $P_{RF} = 0$ W. The particular conditions for this first type were: $I_{Feav} = 600$ mA, $I_{Cuav} = 38$ mA, $Q_{O_2} = 2$ sccm. The second measured type is the hybrid reactive r-HiPIMS + ECWR with applied RF power to ECWR electrode $P_{RF} = 180$ W. The conditions for this second type were: $I_{Feav} = 550$ mA, $I_{Cuav} = 38$ mA, $Q_{O_2} = 2$ sccm. For both these measured types (r-HiPIMS, r-HiPIMS + ECWR) the other parameters were the same, as in case of all deposited samples presented in this paper.

3. Results and Discussion

The results of plasma diagnostics of the reactive r-HiPIMS and hybrid r-HiPIMS + ECWR are in Figures 2 and 3, respectively. The first difference between these two specific cases is the character of discharge current time evolution during the active discharge pulse on the Fe magnetron cathode where the active discharge pulse is quite long (100 μs). In case of pure r-HiPIMS we see typical discharge current decrease after ≈ 30 μs from the beginning of the pulse (Figure 2). This is a typical phenomenon in r-HiPIMS caused by so called gas rarefaction at the surface of the cathode due to the sputtering wind [26]. On the other hand, in case of r-HiPIMS + ECWR, a quite flat discharge current time evolution (Figure 3) can be observed during the active discharge pulse. Similar behavior was already discussed in reference [31] and this effect was explained by higher ionization of the plasma during the active pulse and by higher concentration of double ionized Fe⁺⁺ in r-HiPIMS + ECWR. We have observed difference between r-HiPIMS and r-HiPIMS + ECWR in value and character of time evolution of the ion flux density $i_{ionflux}$ (Figures 2 and 3). In case of r-HiPIMS + ECWR, $i_{ionflux}$ values during active pulses on both cathodes were apparently higher (around 6 mA/cm²) than in case of pure r-HiPIMS where $i_{ionflux} \approx 3$ mA/cm². If we compare the tail electron temperature T_e (Figures 2 and 3), it can be seen that T_e is much higher in case of r-HiPIMS + ECWR than in pure r-HiPIMS. This is important phenomenon of superimposed ECWR plasma because higher T_e means higher probability of ionization of sputtered particles which is the main feature of r-HiPIMS sources. Furthermore, this T_e is very high ($T_e \approx 4$ eV)

during all the time of the “OFF” time period of the pulse in case of hybrid r-HiPIMS + ECWR with measured plasma density $n_i \approx 7 \times 10^{16} \text{ m}^{-3}$ (Figure 3). It means the growing films in hybrid source are interacting with quite intensive plasma during the time between active discharge pulses and this is further significant difference from the pure r-HiPIMS which may influence parameters of deposited film. If we compare the time evolution of measured n_i during active pulses in both cases, Figures 2 and 3, it can be seen that in the iron cathode active discharge pulse n_i decreases from the beginning to the half of the pulse in case of r-HiPIMS + ECWR (Figure 3) and in case of pure r-HiPIMS, n_i gradually increases during all the pulse (Figure 2). During the active discharge pulses of both cathodes, the value of n_i does not significantly differ in hybrid and pure HiPIMS case.

The results of photoelectrochemical measurement of samples 1x, 2x, 3x, and 4x from the Table 1 can be seen in Figure 4. The molar ratios of Cu and Fe measured by XRF for these samples are also in the Table 1. The measured molar ratio was found in the interval between $\frac{n_{\text{Cu}}}{n_{\text{Fe}}} \approx 1.8$ up to $\frac{n_{\text{Cu}}}{n_{\text{Fe}}} \approx 12.3$. This ratio $\frac{n_{\text{Cu}}}{n_{\text{Fe}}}$ is dependent on the ratio of average discharge currents I_{CuAV} and I_{FeAV} but is also strongly dependent on the oxygen flow in plasma Q_{O_2} . It is clear that this oxygen flow strongly influences the sputtering rate of iron target which is partially covered by iron oxide layer which has a smaller sputtering yield. As it can be seen from Table 1, when Q_{O_2} decreased the amount of iron in deposited films strongly increased. In Figure 4a, we can see the linear voltammetry of these samples under light illumination and at dark conditions as the light from the solar simulator is chopped by shutter. All the mentioned samples exhibit the p-type conductivity and have quite large photocurrents. The highest photocurrents can be identified for the sample 2x with the molar ratio $\frac{n_{\text{Cu}}}{n_{\text{Fe}}} = 12.3$, and the highest thickness was 2200 nm. Figure 4b shows the chronoamperometry under the constant illumination by solar simulator for 20 min. The photocurrent at the beginning quickly drops and then very slowly decreases. It looks like the most stable sample from this set of samples is 3x with $\frac{n_{\text{Cu}}}{n_{\text{Fe}}} = 4.3$ and a thickness of 580 nm.

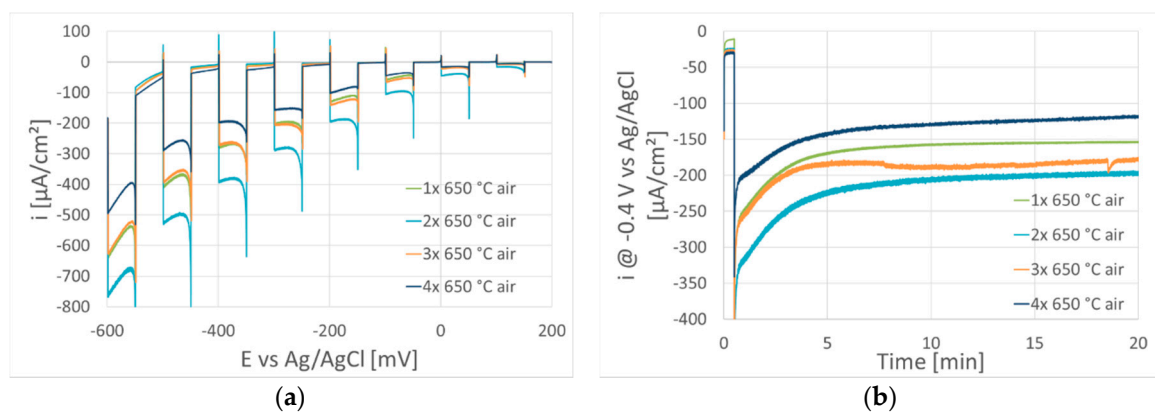


Figure 4. Linear voltammetry (a) and chronoamperometry (b) of films 1x, 2x, 3x, 4x annealed at 650 °C in air for 3 h.

The influence of the presence of oxygen dissolved in electrolyte was studied for sample 2x (Figure S5 in the Supplementary Information). Photoelectrochemical measurement in the absence of oxygen was performed under an argon atmosphere in an electrolyte bubbled by argon for five hours. Measurement in the presence of oxygen was performed under an air atmosphere. It was found that there was an almost negligible decrease in photocurrent in the absence of oxygen. Because of the negligible effect of dissolved oxygen, all photoelectrochemical experiments were done in the presence of oxygen (at concentrations corresponding to the equilibrium with air).

Phase composition of deposited layers 1x–4x changed after post deposition annealing in air or Ar as documented in Figure 5 for samples 1x and 2x. As the deposited sample contains only CuO crystalline phase, after calcination at 650 °C in air, the XRD peak at 45° corresponding to CuO strongly increased as the result of improved crystallinity (see Figure 5a). No other phase than CuO was detected.

On the other side, Cu_2O phase appears when sample (2x) was annealed in the argon atmosphere as can be seen in Figure 5b. The formation of Cu_2O phase can be explained by the reduction of CuO during annealing.

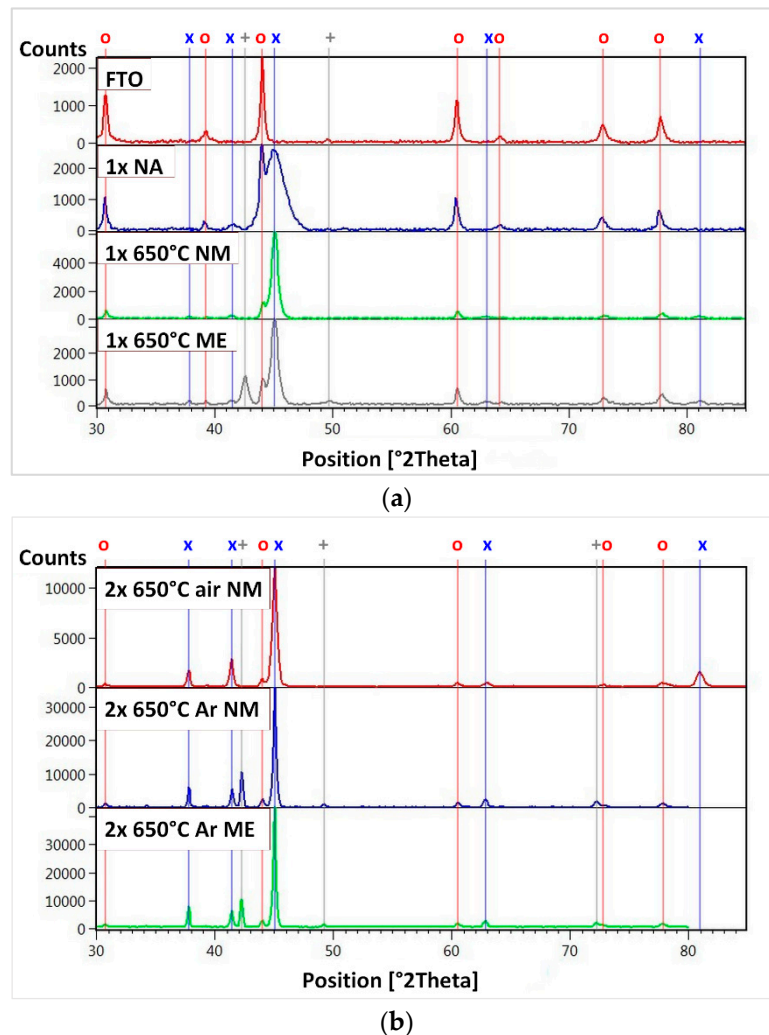


Figure 5. X-ray diffraction (XRD) of fluorine doped tin oxide (FTO) glass and samples 1x (a), 2x (b)—effect of post deposition annealing and photoelectrochemical polarization; \circ SnO_2 ; \times CuO ; $+$ Cu_2O ; NA—as deposited; 650 °C NM—annealed at 650 °C before photoelectrochemical polarization; 650 °C ME—annealed at 650 °C after photoelectrochemical measurement.

The XRD spectra of samples 1x after annealing in air at 650 °C before electrochemical measurement “NM” and after electrochemical measurement “ME” can be also seen in Figure 5a. The sample 1x contains after electrochemical measurement (linear voltammetry and 20 min chronoamperometry at -400 mV vs. Ag/AgCl under light) “ME” also phase Cu_2O (peaks 42.5° and 49.7°). It means that films were slowly reduced during photoelectrochemical measurement. Photocurrents of samples 1x–4x annealed in argon (not shown in graphs) were much lower than samples annealed in air. As can be seen from Table 1, samples 1x–4x have Cu/Fe molar ratio much higher than in the desired delafossite CuFeO_2 (1:1). This is probably the reason why the films 1x–4x contain only CuO and not CuFeO_2 . Furthermore, although samples 1x–4x contain quite significant fraction of Fe no iron or iron oxide phases were identified in these samples. Conditions of the plasma deposition were then further changed and optimized for samples 5x to 10x to achieve the desired molar ratio of $\text{Cu}/\text{Fe} = 1$.

The next investigated series consists of samples 6x, 7x, 8x which were heated during the deposition at 500 °C (Table 1). The results of linear voltammetry and chronoamperometry measurement can be

seen in Figure 6 for sample 6x as deposited and samples 6x, 7x, 8x annealed in air at 650 °C. The ratio of Cu and Fe measured by XRF in these films were in the interval $\frac{n_{Cu}}{n_{Fe}} \approx 0.8 - 1$. The results of XRD measured on the sample 6x without postdeposition annealing, after annealing in air on 650 °C not electrochemically measured “MN” and after annealing in air on 650 °C after photoelectrochemical (PEC) measurement “ME” can be seen in Figure 7. As deposited sample 6x contains delafossite phase (peaks at 36.5° and 72.1°), Cu₂O phase and CuO phase but it does not have any photoresponse in PEC measurement (see Figure 6). After annealing in air, sample 6x lost the delafossite phase which was transformed to CuFe₂O₄ phase, Cu₂O phase disappeared and amount of CuO increased. But annealing in air results in a significant increase in photocurrent response for all samples 6x, 7x and 8x (see Figure 6a), with the highest photocurrents for sample 6x from this set of samples. The chronoamperometry shown in Figure 6b shows that observed photocurrents significantly decrease with time which suggests that these films are not stable in time during PEC polarization. Instability was confirmed by XRD measurement of sample 6 after electrochemical measurement “ME” (Figure 7) which shows the formation of Cu₂O due to the photoelectrochemical reduction of CuO.

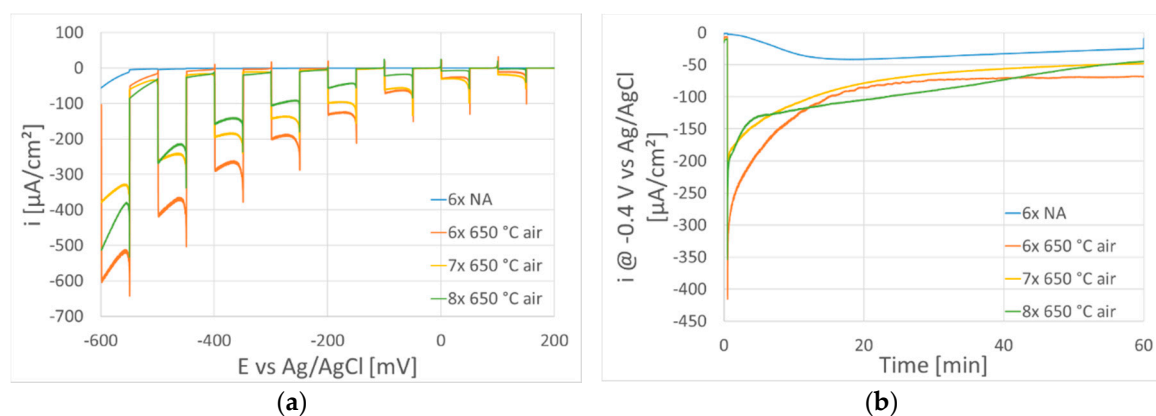


Figure 6. Linear voltammetry (a) and chronoamperometry (b) of samples 6x, 7x, 8x after post deposition annealing in air.

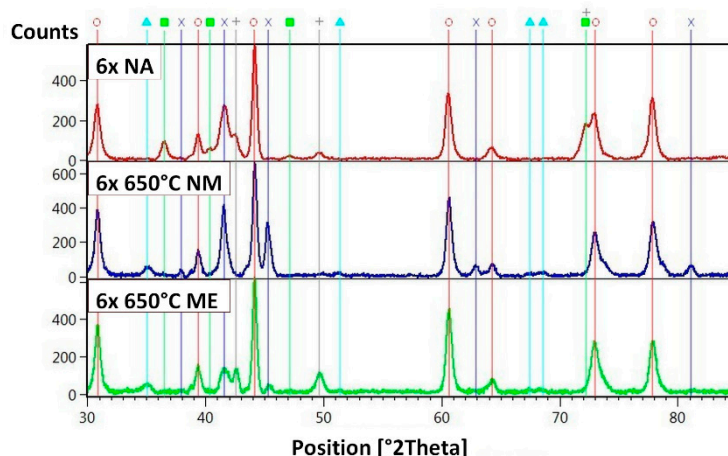


Figure 7. XRD of as deposited (6x) film (NA), after post deposition annealing at 650 °C in air (650 °C NM) and after photoelectrochemical polarization (650 °C ME) ○ SnO₂; × CuO; + Cu₂O; ■ CuFeO₂; ▲ CuFe₂O₄.

In order to get some photocurrents at films with delafossite structure, samples 9x and 10x were annealed after the deposition in vacuum (10^{-3} Pa) at 650 and 500 °C.

Figure S6 (in SI) shows XRD patterns of sample 9x after annealing in a vacuum at 650 °C. After this thermal treatment, sample 9x contains large fraction of delafossite (CuFeO₂) phase and a small amount

of Cu_2O . No other crystal phase containing iron was found. Figure 8 shows chopped light linear voltammetry and chronoamperometry. Chronoamperometry (Figure 8b) of these delafossite samples shows a decrease of photocurrents by time. Although photocurrents obtained from linear voltammetry (Figure 8a) were rather small in comparison with previous set of samples (6x–8x, Figure 6a), it is noticeable that the decrease of photocurrent with polarization time is not as fast as in the case of samples 6x–8x.

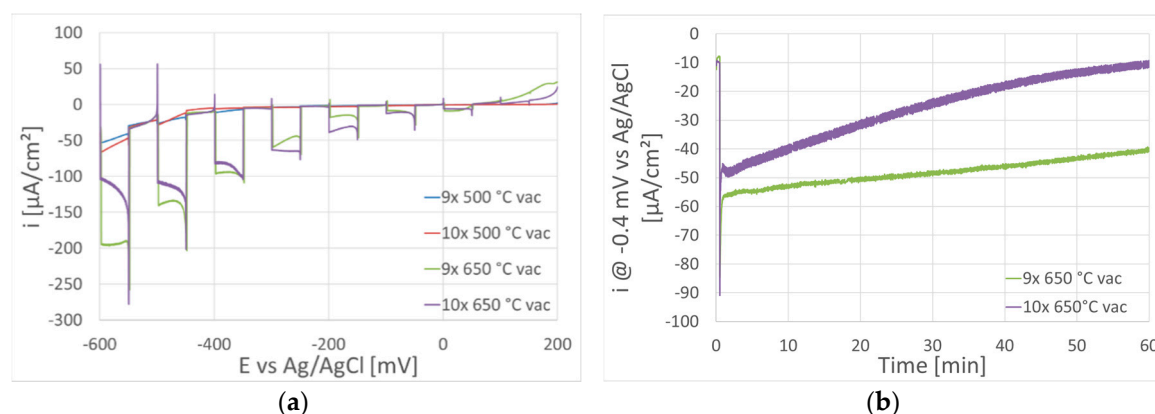


Figure 8. Linear voltammetry (a) and chronoamperometry (b) of samples 9x and 10x exposed to post deposition annealing in vacuum for 6 h at 500 °C (500 °C vac) and 650 °C (650 °C vac).

Table 2 represents the phase composition of samples annealed in vacuum at 650 °C, before (NM) and after (ME) photoelectrochemical polarization. Data are expressed as semiquantitative weight percent phase composition of the measured sample including support FTO glass (SnO_2 phase). There still exist some CuFeO_2 phase after photoelectrochemical polarization, but phase composition for each sample is different. While sample 9x contains a smaller amount of CuFeO_2 , an increased amount of Cu_2O , and a new phase Fe_3O_4 , sample 10x contains similar amount of CuFeO_2 , and Cu_2O disappears. This means that sample 9x contains CuFeO_2 , which is stable during photoelectrochemical polarization and at the same time exhibits promising photocurrent values. Further work will be devoted to the deposition of films with higher content of CuFeO_2 at deposition conditions corresponding to sample 9x to achieve more efficient and stable p-type photocathode films.

Table 2. Semiquantitative XRD analysis.

Phase	Semiquantitative Phase Composition/%			
	9x 650 °C vac NM	9x 650 °C vac ME	10x 650 °C vac NM	10x 650 °C vac ME
CuFeO_2	67	29	80	100
Cu_2O	33	43	20	–
Fe_3O_4	–	28	–	–

The results of measurement of optical transmission in UV-VIS region can be seen in Figure 9 for particular deposited samples. The optical band gap can only be roughly estimated because we used only transmission spectra. All optical diagnostics was done on the films before PEC measurements. The right graph shows also optical transmission of bare FTO glass after annealing on 650 °C. It can be seen that FTO glass is still very well transparent up to 3.5 eV. The molar ratio of Cu/Fe is mentioned at each optical spectrum. Samples in the left graph 2x–5x were all annealed in air up to 650 °C. As it was shown from the diffraction experiment, sample 2x with the molar ratio $n_{\text{Cu}}/n_{\text{Fe}} = 12.5$ exhibits the crystal structure of CuO (Figure 5). For the sample 2x the band gap was $E_g \approx 1.5$ eV, which is close to reported value of CuO crystalline material [38]. When the iron amount grows in the films the band gap increases to the values close to $E_g \approx 2$ eV. On the right graph we can see transmission spectra of samples

9x, 10x annealed in vacuum on 650 °C, and these samples contain a large fraction of delafossite phase (Table 2). Samples 9x and 10x with the highest amount of delafossite phase have the band gap $E_g \approx 1.8$ eV, this is in the region typically reported for delafossite [4]. These two samples have also $n_{Cu}/n_{Fe} \approx 1$.

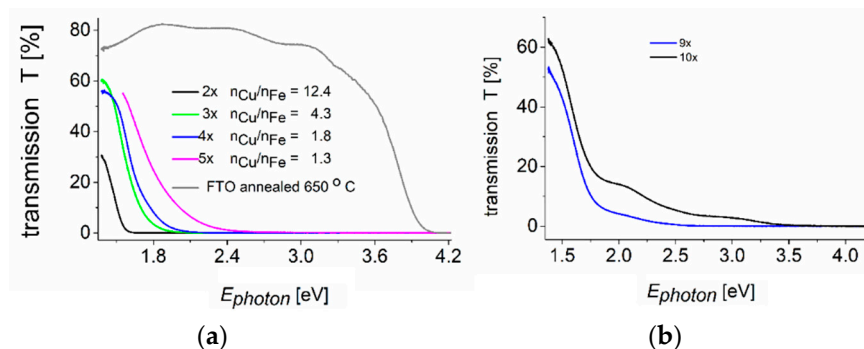


Figure 9. Transmission spectra of selected deposited films 2x, 3x, 4x, 5x (a) and 9x, 10x (b) on FTO glass substrates measured by UV-VIS optical spectrometry. All optical diagnostics was done on the films before PEC measurements.

4. Conclusions

A reactive high-power impulse magnetron sputtering system (r-HiPIMS) and a hybrid high power impulse magnetron sputtering combined with electron cyclotron wave resonance plasma source (r-HiPIMS + ECWR) were used for the deposition of p-type $CuFe_xO_y$ thin films onto FTO substrates.

These experiments confirm that at certain conditions in this r-HiPIMS and in hybride r-HiPIMS + ECWR reactive sputtering process a delafossite $CuFeO_2$ phase can be formed in the deposited material after the post deposition annealing in vacuum. On the other hand, the material still contains different phases like Cu_2O or some phases of iron oxides. For this reason, the stability of prepared cathodes was still limited. For future experiments, more precise stoichiometry control of the sputtering rate of copper and iron should be implemented, together with some emission spectroscopy measurements of Cu and Fe atoms in the magnetron plasma. Furthermore, more stable and thermal resistant substrates with conductive electrode should be used for deposition experiments. Deposition conditions were optimized to achieve the desired Cu/Fe ratio = 1 in deposited films, as deposited films have negligible photocurrent response. Annealing in 650 °C results in photoactive films where the p-type material is CuO. However, the photocurrent decreases with the time of the photoelectrochemical polarization due to the reduction of CuO to Cu_2O . High temperature of deposition (500 °C) together with post deposition heat treatment at 650 °C in vacuum is essential for the formation of stable and photoactive $CuFeO_2$ phase. Further effort will be devoted to increase $CuFeO_2$ content and to achieve more efficient p-type photocathode films.

Supplementary Materials: The following are available online at <http://www.mdpi.com/2079-6412/10/3/232/s1>, Figure S1: Experimental configuration of guarded planar radio frequency (RF) probe for measurement of current and voltage waveforms and plasma diagnostics, Figure S2: The example of time evolution of RF current IRFprobe RF voltage URFprobe measured on the RF planar probe. Time evolution of cathode voltage on Cu cathode is shown as well in case of reactive r-HiPIMS + ECWR deposition copper iron oxide with PECWR = 180 W, Figure S3: Example of reconstructed current voltage characteristics for the single U_{RFp} voltage sweep in the middle of copper discharge pulse in case of reactive r-HiPIMS + ECWR deposition copper iron oxide with PECWR = 180 W, Figure S4: Example of reconstructed current voltage characteristics for the single U_{RFp} voltage sweep in the middle of copper pulse in case of reactive r-HiPIMS + ECWR deposition copper iron oxide with PECWR = 180 W, logarithm of second derivative is shown with fitted electron temperature Te from the tail of electron distribution function, Figure S5: Linear voltammety of the sample 2x annealed in air on 650 °C in electrolyte without degassing by argon and in electrolyte degassed by flow of argon for 5 h before PEC measurement, Figure S6: X-ray diffraction (XRD) of sample 9x with significant delafossite structure after annealing of the sample after deposition on 650 °C in vacuum.

Author Contributions: Z.H. was involved in writing of original draft manuscript and its revision, he also performed thin film deposition, M.Z. was involved in film characterization, photoelectrochemical measurement and data analysis, J.O. performed thin film analysis, D.T. and M.Č. were involved in plasma diagnostics and J.K. managed literature search and contributed to writing of original manuscript and its revision. All authors have read and agreed to the published version of the manuscript.

Funding: This work was supported by project no. 17-20008S of the Grant Agency of the Czech Republic. The work was also supported by project MPO TRIO II no. FV20580 and by the Operational Programme Research, Development and Education financed by the European Structural and Investment Funds and the Czech Ministry of Education, Youth and Sports (Project No. SOLID21 - CZ.02.1.01/0.0/0.0/16_019/0000760).

Conflicts of Interest: The authors declare no conflict of interest.

References

1. Xiong, L.; Huang, S.; Yang, X.; Qiu, M.; Chen, Z.; Yu, Y. p-Type and n-type Cu_2O semiconductor thin films: Controllable preparation by simple solvothermal method and photoelectrochemical properties. *Electrochim. Acta* **2011**, *56*, 2735–2739. [[CrossRef](#)]
2. Paracchino, A.; Mathews, N.; Hisatomi, T.; Stefiik, M.; Tilley, S.D.; Gratzel, M. Ultrathin films on copper(I) oxide water splitting photocathodes: A study on performance and stability. *Energy Environ. Sci.* **2012**, *5*, 8673–8681. [[CrossRef](#)]
3. Panah, S.M.; Moakhar, R.S.; Chua, C.S.; Kushwaha, A.; Dalapati, G.K. Stable and efficient CuO based photocathode through oxygen-rich composition and Au-Pd nanostructure incorporation for solar-hydrogen production. *ACS Appl. Mater. Interfaces* **2017**, *9*, 27596–27606. [[CrossRef](#)] [[PubMed](#)]
4. Crespo, C.T. Potentiality of CuFeO_2 -delafossite as a solar energy converter. *Solar Energy* **2018**, *163*, 162–166. [[CrossRef](#)]
5. Prevot, M.S.; Guijarro, N.; Sivula, K. Enhancing the performance of a robust sol-gel-processed p-type delafossite CuFeO_2 photocathode for solar water reduction. *ChemSusChem* **2015**, *8*, 1359–1367. [[CrossRef](#)] [[PubMed](#)]
6. Husek, J.; Cirri, A.; Biswas, S.; Asthagiri, A.; Baker, L.R. Hole thermalization dynamics facilitate ultrafast spatial charge separation in CuFeO_2 solar photocathodes. *J. Phys. Chem. C* **2018**, *122*, 11300–11304. [[CrossRef](#)]
7. Du, F.; Chen, Q.; Wang, Y. Effect of annealing process on the heterostructure $\text{CuO/Cu}_2\text{O}$ as a highly efficient photocathode for photoelectrochemical water reduction. *J. Phys. Chem. Solids* **2017**, *104*, 139–144. [[CrossRef](#)]
8. Rahman, M.; MacElroy, J.M.D.; Dowling, D.P. Influence of the physical, structural and chemical properties on the photoresponse property of magnetron sputtered TiO_2 for the application of water splitting. *J. Nanosci. Nanotechnol.* **2011**, *11*, 8642–8651. [[CrossRef](#)]
9. Krýsa, J.; Nemečková, A.; Zlámál, M.; Kotrla, T.; Baudys, M.; Kment, Š.; Hubička, Z.; Neumann-Spallart, M. $\alpha\text{-Fe}_2\text{O}_3/\text{TiO}_2$ stratified photoanodes. *J. Photochem. Photobiol. A Chem.* **2018**, *366*, 12–17. [[CrossRef](#)]
10. Jia, L.; Harbauer, K.; Bogdanoff, P.; Ellmer, K.; Fiechter, S. Sputtering deposition of ultra-thin $\alpha\text{-Fe}_2\text{O}_3$ films for solar water splitting. *J. Mater. Sci. Technol.* **2015**, *31*, 655–659. [[CrossRef](#)]
11. Horiuchi, Y.; Mine, S.; Moriyasu, M.; Anpo, M.; Kim, T.H.; Matsuoka, M. Preparation of tantalum oxynitride thin film photocatalysts by reactive magnetron sputtering deposition under high substrate temperature. *Res. Chem. Intermed.* **2017**, *43*, 5123–5136. [[CrossRef](#)]
12. Marsen, B.; Miller, E.L.; Paluselli, D.; Rocheleau, R.E. Progress in sputtered tungsten trioxide for photoelectrode applications. *Int. J. Hydrog. Energy* **2007**, *32*, 3110–3115. [[CrossRef](#)]
13. Olejníček, J.; Brunclíková, M.; Kment, Š.; Hubička, Z.; Kmentová, H.; Kšířová, P.; Čada, M.; Zlámál, M.; Krýsa, J. WO_3 thin films prepared by sedimentation and plasma sputtering. *Chem. Eng. J.* **2017**, *318*, 281–288. [[CrossRef](#)]
14. Hubička, Z.; Zlámál, M.; Čada, M.; Kment, Š.; Krýsa, J. Photo-electrochemical stability of copper oxide photocathodes deposited by reactive high power impulse magnetron sputtering. *Catal. Today* **2019**, *328*, 29–34. [[CrossRef](#)]
15. Patel, M.; Kim, H.S.; Patel, D.B.; Kim, J. CuO photocathode-embedded semitransparent photoelectrochemical cell. *J. Mater. Res.* **2016**, *31*, 3205–3213. [[CrossRef](#)]
16. Xie, T.; Zheng, T.; Wang, R.; Bu, Y.; Ao, J.P. Fabrication of CuO_x thin-film photocathodes by magnetron reactive sputtering for photoelectrochemical water reduction. *Green Energy Environ.* **2018**, *3*, 239–246. [[CrossRef](#)]

17. Jiang, C.M.; Reyes-Lillo, S.E.; Liang, Y.; Liu, Y.S.; Liu, G.; Toma, F.M.; Prendergast, D.; Sharp, I.D.; Cooper, J.K. Electronic structure and performance bottlenecks of CuFeO₂ photocathodes. *Chem. Mater.* **2019**, *31*, 2524–2534. [[CrossRef](#)]
18. Vasina, P.; Fekete, M.; Hnilica, J.; Klein, P.; Dosoudilova, L.; Dvorak, P.; Navratil, Z. Determination of titanium atom and ion densities in sputter deposition plasmas by optical emission spectroscopy. *Plasma Sources Sci. Technol.* **2015**, *24*, 065022. [[CrossRef](#)]
19. Ehiasarian, A.P.; Gonzalvo, Y.A.; Whitmore, T.D. Time-resolved ionisation studies of the high power impulse magnetron discharge in mixed argon and nitrogen atmosphere. *Plasma Process. Polym.* **2007**, *4*, S309–S313. [[CrossRef](#)]
20. Peng, W.C.; Chen, Y.C.; He, J.L.; Ou, S.L.; Horng, R.H.; Wu, D.S. Tunability of p- and n-channel TiO_x thin film transistors. *Sci. Rep.-UK* **2018**, *8*, 9255. [[CrossRef](#)]
21. Tiron, V.; Velicu, I.L.; Stanescu, D.; Magnan, H.; Sirghi, L. High visible light photocatalytic activity of nitrogen-doped ZnO thin films deposited by HiPIMS. *Surf. Coat Technol.* **2017**, *324*, 594–600. [[CrossRef](#)]
22. Cemin, F.; Tsukamoto, M.; Keraudy, J.; Antunes, V.G.; Helmersson, U.; Alvarez, F.; Minea, T.; Lundin, D. Low-energy ion irradiation in HiPIMS to enable anatase TiO₂ selective growth. *J. Phys. D Appl. Phys.* **2018**, *51*, 235301. [[CrossRef](#)]
23. Kouznetsov, V.; Macák, K.; Schneider, J.M.; Helmersson, U.; Petrov, I. A novel pulsed magnetron sputter technique utilizing very high target power densities. *Surf. Coat. Technol.* **1999**, *122*, 290–293. [[CrossRef](#)]
24. Helmersson, U.; Lattemann, M.; Bohlmarm, J.; Ehiasarian, A.P.; Gudmundsson, J.T. Ionized physical vapor deposition (IPVD): A review of technology and applications. *Thin Solid Films* **2006**, *513*, 1–24. [[CrossRef](#)]
25. Cemin, F.; Abadias, G.; Minea, T.; Furgeaud, C.; Brisset, F.; Solas, D.; Lundin, D. Benefits of energetic ion bombardment for tailoring stress and microstructural evolution during growth of Cu thin films. *Acta Mater.* **2017**, *141*, 120–130. [[CrossRef](#)]
26. Anders, A. Tutorial: Reactive high power impulse magnetron sputtering (R-HiPIMS). *J. Appl. Phys.* **2017**, *121*, 171101. [[CrossRef](#)]
27. Anders, A.; Čapek, J.; Hála, M.; Martinu, L. The ‘recycling trap’: A generalized explanation of discharge runaway in high-power impulse magnetron sputtering. *J. Phys. D Appl. Phys.* **2012**, *45*, 012003. [[CrossRef](#)]
28. Poolcharuansin, P.; Bowes, M.; Petty, T.J.; Bradley, J.W. Ionized metal flux fraction measurements in HiPIMS discharges. *J. Phys. D Appl. Phys.* **2012**, *45*, 322001. [[CrossRef](#)]
29. Straňák, V.; Herrendorf, A.P.; Drache, S.; Čada, M.; Hubička, Z.; Tichý, M.; Hippler, R. Highly ionized physical vapor deposition plasma source working at very low pressure. *Appl. Phys. Lett.* **2012**, *100*, 141604. [[CrossRef](#)]
30. Straňák, V.; Herrendorf, A.P.; Drache, S.; Čada, M.; Hubička, Z.; Bogdanowicz, R.; Tichy, M.; Hippler, R. Plasma diagnostics of low pressure high power impulse magnetron sputtering assisted by electron cyclotron wave resonance plasma. *J. Appl. Phys.* **2012**, *112*, 093305. [[CrossRef](#)]
31. Straňák, V.; Hubička, Z.; Čada, M.; Drache, S.; Tichý, M.; Hippler, R. Investigation of ionized metal flux in enhanced high power impulse magnetron sputtering discharges. *J. Appl. Phys.* **2014**, *115*, 153301. [[CrossRef](#)]
32. Straňák, V.; Herrendorf, A.P.; Wulff, H.; Drache, S.; Čada, M.; Hubička, Z.; Tichý, M.; Hippler, R. Deposition of rutile (TiO₂) with preferred orientation by assisted high power impulse magnetron sputtering. *Surf. Coat. Technol.* **2013**, *222*, 112–117. [[CrossRef](#)]
33. Straňák, V.; Hubička, Z.; Čada, M.; Bogdanowicz, R.; Wulff, H.; Helm, C.A.; Hippler, R. Influence of reactive oxygen species during deposition of iron oxide films by high power impulse magnetron sputtering. *J. Phys. D Appl. Phys.* **2018**, *51*, 095205. [[CrossRef](#)]
34. Sezemský, P.; Straňák, V.; Kratochvíl, J.; Čada, M.; Hippler, R.; Hrabovský, M.; Hubicka, Z. Modified high frequency probe approach for diagnostics of highly reactive plasma. *Plasma Sources Sci. Technol.* **2019**, *28*, 115009. [[CrossRef](#)]
35. Sobolewski, M.A. Measuring the ion current in electrical discharges using radio-frequency current and voltage measurements. *Appl. Phys. Lett.* **1998**, *72*, 1146–1148. [[CrossRef](#)]
36. Sobolewski, M.A. Measuring the ion current in high-density plasmas using radio-frequency current and voltage measurements. *J. Appl. Phys.* **2001**, *90*, 2660. [[CrossRef](#)]

37. Sobolewski, M.A.; Lahr, D.L. Origin of electrical signals for plasma etching end point detection: Comparison of end point signals and electron density. *Vac. Sci. Technol. A* **2012**, *30*, 051303. [[CrossRef](#)]
38. Murali, D.S.; Kumar, S.; Choudhary, R.J.; Wadikar, A.D.; Jain, M.K.; Subrahmanyam, A. Synthesis of Cu₂O from CuO thin films: Optical and electrical properties. *AIP Adv.* **2015**, *5*, 047143. [[CrossRef](#)]



© 2020 by the authors. Licensee MDPI, Basel, Switzerland. This article is an open access article distributed under the terms and conditions of the Creative Commons Attribution (CC BY) license (<http://creativecommons.org/licenses/by/4.0/>).